Journal of Catalysis **210,** 319–327 (2002)
doi:10.1006/jcat.2002.3674

# Hydrodesulfurization of Dibenzothiophene over Siliceous MCM-41-Supported Catalysts

## II. Sulfided Ni–Mo Catalysts

Anjie Wang,*,[1] Yao Wang,* Toshiaki Kabe,† Yongying Chen,* Atsushi Ishihara,† Weihua Qian†, and Pingjing Yao*

**State Key Laboratory of Fine Chemicals, Dalian University of Technology, 158 Zhongshan Road, Dalian, 116012, People's Republic of China; and †Department of Applied Chemistry, Faculty of Technology, Tokyo University of Agriculture and Technology, 2-24-16 Nakacho, Koganei, Tokyo 184, Japan*

Received January 16, 2002; revised May 14, 2002; accepted May 17, 2002

**High-performance hydrodesulfurization (HDS) catalysts were prepared by depositing Ni–Mo species over siliceous MCM-41. HDS of dibenzothiophene (DBT), one of the most refractory sulfur-containing molecules in petroleum, was used to evaluate the activity of the prepared catalysts. The Ni–Mo/MCM-41 showed better performance than the Co–Mo/MCM-41 in the HDS of DBT, probably due to the enhanced hydrogenation ability of Ni–Mo sulfides. The selectivities of the products indicated that both hydrogenolysis and hydrogenation followed by desulfurization play important roles in HDS of DBT, in contrast with the results of HDS of DBT catalyzed by Co–Mo/MCM-41. The optimum HDS activity was observed at a Ni/Mo atomic ratio of 0.75, similar to that of Co–Mo/MCM-41 catalysts but higher than the conventional $\gamma$-$Al_2O_3$-supported catalysts. The higher optimal Ni/Mo ratio may be attributed to the higher dispersion of the active species and to generation of more Ni–Mo pairs on the surface of MCM-41. The high performance of the prepared Ni–Mo(0.75)/MCM-41 catalyst was confirmed by the HDS of 4-methyldibenzothiophene, 4,6-dimethyldibenzothiophene, and a high-sulfur diesel. The $^{35}S$ isotope tracer investigation revealed that sulfur atoms accommodated on the surface after HDS could be released only by the introduction of a sulfur-containing compound, indicating that sulfur-atom exchange between sulfur-containing molecules and the active sites is involved in the HDS reaction. Accordingly, a reaction mechanism for HDS is proposed.**



*Key Words:* **hydrodesulfurization; MCM-41; Ni–Mo sulfides; dibenzothiophene; mechanism.**

### 1. INTRODUCTION

Hydrodesulfurization (HDS) is a key process used in producing clean engine fuels. In the process, alumina-supported CoMoS, NiMoS, and NiWS phases are traditionally used as catalysts. However, new types of catalysts with significantly improved catalytic performance must be developed to satisfy future environmental legislation. Since cobalt- or nickel-promoted molybdenum/tungsten sulfides are basically established as the active species for the commercial HDS catalyst, developing better supports are important for developing high-performance HDS catalysts.

Mesoporous MCM-41 has been the focus of much research interest since its discovery because it offers a uniform pore of 15 to 100 Å and a specific surface area of over 1000 $cm^2/g$ (1). Shortly after the discovery of MCM-41, Corma *et al.* (2) used Al/MCM-41 to support Ni–Mo species to prepare catalysts for hydrocracking of vacuum gas oil. They found that Al/MCM-41-supported catalysts were more active in HDS, hydrodenitrogenation (HDN), and hydrocracking than those supported over USY (Ultra-Stable Y zeolite) or $\gamma$-$Al_2O_3$. Song and Reddy (3, 4) supported Co–Mo and Ni–Mo over Al/MCM-41 to investigate the HDS of dibenzothiophene (DBT), and petroleum, atmospheric, and vacuum residues. They reported that the Al/MCM-41-supported catalysts showed higher performance in deep HDS than the $\gamma$-$Al_2O_3$-supported catalysts. Landau *et al.* achieved a much higher loading when depositing Co–Mo species on Al/MCM-41 by ultrasonic treatment. They found that the high-loading Co–Mo/Al/MCM-41 catalysts were 1.7 times more active than a commercial catalyst in HDS of DBT (5). It is interesting to note that most research has focused on Al/MCM-41, probably in expectation that the strong acidity of the support may help to crack the polyaromatic sulfur-containing compounds in order to improve the HDS activity.

However, Ramíre *et al.* (6) reported that the strong acidity of the support ($Al_2O_3$ + MCM-41) was detrimental to the HDS activity of the catalysts. They believe that only weak and medium acids on the surface favor the formation of HDS active sites.

[1] To whom correspondence should be addressed. E-mail: anjwang@chem.dlut.edu.cn.



0021-9517/02 $35.00

In previous work (7, 8), we reported that the siliceous MCM-41-supported Co–Mo or Ni–W sulfides showed significant improvement in the HDS of DBT, a refractory molecule in petroleum. It seems that the improvement in the HDS catalytic activity can be attributed to the high surface area and the mild acidity of the support.

In the present study, the HDS of DBT over Ni–Mo catalysts supported by siliceous MCM-41 was investigated. The HDS reactions of 4-methyldibenzothiophene (4-MDBT), 4,6-dimethyldibenzothiophene (4,6-DMDBT), and a high-sulfur-containing straight-run diesel were conducted to evaluate the HDS performance of the prepared catalysts. The radioisotope tracer method was used to trace the dynamic behavior of sulfur atoms during HDS to elucidate the mechanism of HDS reaction.

## 2. METHODS

### 2.1. Materials

Both ammonium heptamolybdate tetrahydrate $[(NH_4)_6 Mo_7O_{24} \cdot 4H_2O]$ and nickel nitrate hexahydrate $[Co(NO_3)_2 \cdot 6H_2O]$ were of commercial GR grade (Kishida Chemicals). DBT ($[^{32}S]$DBT) was the product of Acros Organics. 4-MDBT and 4,6-DMDBT were synthesized according to methods in the literature (9, 10). Decalin, obtained from Kishida Chemicals, was used as solvent without further purification. Hydrogen (99.99%) was supplied by Tohei Chemicals, and hydrogen sulfide in hydrogen ($H_2S$ 5.0%) was supplied by Takachio Chemicals. The synthesis of $[^{35}S]$DBT and the preparation of siliceous MCM-41 were described in a previous paper (7). A high-sulfur-containing straight-run diesel (2.83 wt% S) was sampled from a distillation system (Dalian West Pacific Petrochemical Co.).

### 2.2. Catalysts

Siliceous MCM-41-supported Ni–Mo catalysts were prepared by the wet impregnation method described in a previous paper (7). A loading level of 20 wt% $MoO_3$ was chosen for this series of catalysts and the loading of NiO was determined by the Ni–Mo atomic ratio. The prepared catalysts were denoted as Ni–Mo(x). The value in parentheses represents the Ni–Mo atomic ratio.

Nitrogen adsorption on siliceous MCM-41 and its supported catalysts was performed using a Quantachrome adsorption analyzer, which reports sorption isotherms, BET specific surface area, and pore volume automatically. The samples were outgassed for 4 h at 300°C before the adsorption. The reduction behavior was determined by temperature-programmed reduction (TPR) with $H_2$. The TPRs of the Ni–Mo catalysts were measured on a ChemBET 3000 analyzer. Before the measurement, the sample was treated in argon at 200°C for 2 h. A gas mixture of $H_2$ and Ar (5 vol% $H_2$ in argon) was used as the reagent. The TPR patterns of the catalysts were measured from room temperature to 930°C at 10°C/min. The $NH_3$-TPD data were collected using a ChemBET 3000 analyzer. About 200 mg of sample was activated in flowing He at 500°C for 2 h, then cooled to 120°C under continuous evacuation. The sample was equilibrated with gaseous $NH_3$ at 0.04 kPa. The reactor temperature was ramped up at a rate of 10°C/min while He flow was passed through the reactor at 20 $cm^3$/min.

### 2.3. System and Procedure for HDS and Isotope Tracer Experiments

HDS reactions of DBT, 4-MDBT, 4,6-DMDBT, and a straight-run diesel were performed in a trickle-bed reactor with an 8.0-mm internal diameter. The procedures of presulfidation, HDS, and isotope tracer experiments were described in detail in a previous paper (7).

The HDS activities of the prepared catalysts were evaluated using the following model fuels: 1 wt% DBT in decalin, 0.5 wt% 4-MDBT in decalin, and 0.5 wt% 4,6-DMDBT in decalin. The reaction was carried out under the following conditions: temperature of 260–380°C, total pressure of 5.0 MPa, $H_2$/feed ratio of 1200 $Nm^3/m^3$, and WHSV of 45 $h^{-1}$. The products were analyzed using GC (Shimazu 17A). The performance of the prepared catalysts was verified by the HDS of a high-sulfur-containing straight-run diesel. The HDS conditions were temperature of 320°C, total pressure of 5.0 MPa, $H_2$/feed ratio of 1200 $Nm^3/m^3$, and WHSV of 2 $h^{-1}$. The sulfur contents of the feed and the product were analyzed by an XRF analyzer (Bruker RSR 3400 X).

### 2.4. Measurement of Catalyst Activity

The activities of HDS of DBT, hydrogenolysis (HGY), hydrogenation and desulfurization (HYD), and hydrocracking (HYC) were estimated by the analysis of the liquid products, based on the well-established reaction path network of DBT HDS (7). Their pseudo-first-order rate constants were determined by

$$k_{HDS} = \frac{-\ln(1-x)\cdot m \cdot F}{A},$$
$$k_{HYG} = k_{HDS} \cdot S_{BP},$$
$$k_{HYD} = k_{HDS} \cdot S_{CHB},$$
$$k_{HYC} = k_{HDS} \cdot S_{B+C}/2,$$

where $x$ is the conversion of DBT, $m$ is the charge weight of the catalyst (g), $F$ is the feed rate of DBT (atom/s), and $A$ is the specific surface area ($nm^2$/g). $S_{BP}$, $S_{CHB}$, and $S_{B+C}$ represent the selectivities of biphenyl (BP), cyclohexylbenzene (CHB), and the combination of benzene and cyclohexane, respectively.

In the case of the HDS of 4-MDBT, 4,6-DMDBT, or diesel, the conversion of sulfur-containing reactants was used to measure the HDS performance of the catalyst.

## 3. RESULTS

### *3.1. Characterization of MCM-41 and Its Supported Catalysts*

The $N_2$ adsorption–desorption isotherms of the prepared siliceous MCM-41-supported Ni–Mo catalysts are shown in Fig. 1. They are typical type-IV isotherms. At low relative pressure, the $N_2$ uptake increases sharply as the $N_2$ pressure increases, which indicates that the support has a very high surface area. In addition, there is another sharp increase in the range of $P/P_0 = 0.3$–$0.4$ in the isotherms. This sharp increase in uptake results from the capillary condensation of $N_2$, which suggests that uniform mesopores are present in the siliceous MCM-41. All the isotherms are type-IV shapes, but the uptake of $N_2$ decreases with the loading of the metal species. The deposition of metal species leads to the reduction of $N_2$ adsorption on the surface, probably due to blocking of pores. However, it is worth noting that Ni/MCM-41 showed highest adsorption among all the MCM-41-supported catalysts, suggesting that chemical adsorption of $N_2$ on Ni species may occur.

The physical properties of the prepared catalysts are summarized in Table 1. It is shown that both BET specific surface area and pore volume of catalysts were reduced after being deposited by the metal species. The decreases in specific surface area and pore volume result partly from the density increase of the catalysts and partly from the pore-blocking by the metal species.

**TABLE 1**

**Physical Properties of Siliceous MCM-41 and Its Supported Catalysts**

| Catalyst | BET surface area ($m^2/g$) | Pore volume ($cm^3/g$) | Mo content ($atom/nm^2$) | Ni content ($atom/nm^2$) |
|---|---|---|---|---|
| MCM-41 | 1046 | 1.00 | — | — |
| Mo/MCM-41 | 628 | 0.61 | 1.33 | — |
| Ni–Mo(0.25) | 805 | 0.72 | 1.04 | 0.26 |
| Ni–Mo(0.50) | 698 | 0.65 | 1.20 | 0.60 |
| Ni–Mo(0.75) | 660 | 0.67 | 1.27 | 0.95 |
| Ni–Mo(1.00) | 608 | 0.43 | 1.38 | 1.38 |
| Ni–Mo(1.25) | 543 | 0.38 | 1.54 | 1.92 |
| Ni/MCM-41 | 888 | 0.98 | — | 1.82 |

The TPR profiles of siliceous MCM-41 and its supported catalysts are illustrated in Fig. 2. For comparison, The TPR profile of Ni–Mo/$\gamma$-$Al_2O_3$ with a Ni/Mo atomic ratio of 0.75 was also measured. The $H_2$-consumption temperature peaks are summarized in Table 2. There is one

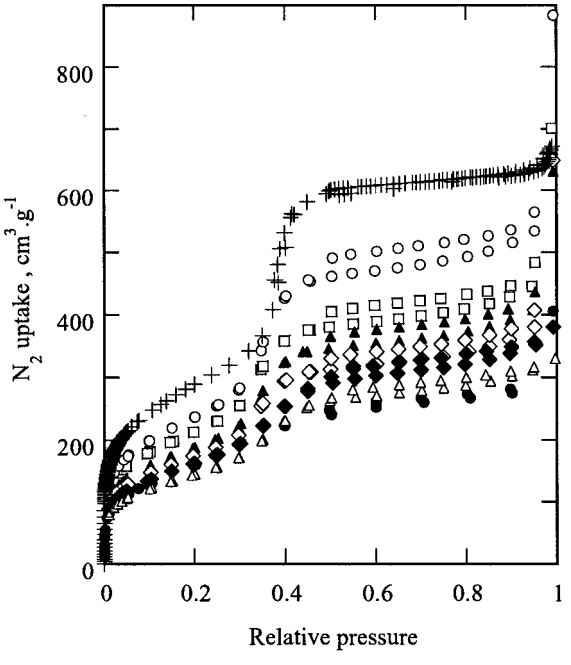


**FIG. 1.** $N_2$ adsorption–desorption isotherms of siliceous MCM-41 and its supported catalysts: (+), MCM-41; (○), Ni/MCM-41; (●), Mo/MCM-41; (□), Ni–Mo(0.25); (▲), Ni–Mo(0.50); (◇), Ni–Mo(0.75); (◆), Ni–Mo(1.00); (△), Ni–Mo(1.25).

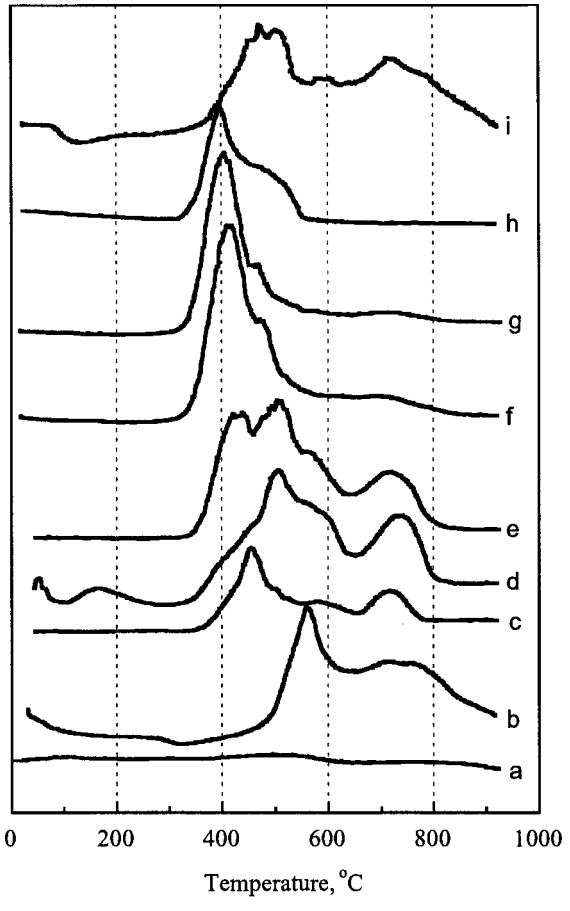


**FIG. 2.** TPR profiles of siliceous MCM-41 and its supported catalysts: (a) MCM-41, (b) Mo/MCM-41, (c) Ni–Mo(0.25), (d) Ni–Mo(0.50), (e) Ni–Mo(0.75), (f) Ni–Mo(1.00), (g) Ni–Mo(1.25), (h) Ni/MCM-41, (i) Ni–Mo(0.75)/$\gamma$-$Al_2O_3$.

**TABLE 2**

**Main Reduction Temperatures in the TPR Profiles of Supported NiMo Catalysts**

| Catalyst | Main reduction temperature[a] (°C) |
|---|---|
| $MoO_3$ | 562, 752 |
| Ni–Mo(0.25) | 454, 716 |
| Ni–Mo(0.50) | 506, 584, 738 |
| Ni–Mo(0.75) | 438, 493, 556, 720 |
| Ni–Mo(0.75)/$\gamma$-$Al_2O_3$ | 450, 465, 603, 723 |
| Ni–Mo(1.00) | 411, 470 |
| Ni–Mo(1.25) | 405, 468 |
| NiO | 398 |

[a] Number of values indicates number of $H_2$-consumption peaks for the respective species.

peak around 400°C with a shoulder for $H_2$ consumption for Ni/MCM-41 while there are two $H_2$-consumption peaks above 500°C for Mo/MCM-41, indicating that the reducibility of Ni species is superior to that of Mo species. Since the reduction of supported $MoO_3$ species involves two steps ($MoO_3 \rightarrow MoO_2 \rightarrow Mo$), the former peak can be attributed to reduction of $Mo^{6+}$ to $Mo^{4+}$, and the latter to reduction of $Mo^{4+}$ to Mo (11).

As the Ni/Mo atomic ratio increases, the characteristic reduction temperature of the Mo site shifts to lower temperature, suggesting a strong interaction between Ni and Mo species. Moreover, the lower temperature reduction peak splits into two or three peaks while the reduction peak at higher temperature is enhanced as the Ni/Mo atomic ratio increases, suggesting that some intermediate species may be formed. However, the split peaks and the enhanced peak disappear when the Ni/Mo atomic ratio reaches 1.0 or above. The shift, split, and disappearance of the Mo reduction peaks by the introduction of Ni species may have resulted from the interaction between the metal species, and from the hydrogen spillover from Ni sites to Mo sites on the surface of the support.

Four reduction peaks appear in the TPR profile of Ni–Mo(0.75)/$\gamma$-$Al_2O_3$, similar to that of Ni–Mo(0.75)/MCM-41. However, there exist some differences in reduction peak temperatures and in the peak intensity. The similarity between both TPR profile shapes suggests that the interaction between Ni and Mo species may play an important role in determining the cause of the reduction peak split at lower temperature. The differences in the reduction peak temperatures may result from the interaction between metal species and the supports. At higher temperatures, no noticeable shift of the reduction peak was observed, but the peak intensity of Ni–Mo(0.75)/MCM-41 was stronger than that of Ni–Mo(0.75)/$\gamma$-$Al_2O_3$.

The $NH_3$-TPD profile of siliceous MCM-41 compared with $\gamma$-$Al_2O_3$, is shown in Fig. 3. It is indicated that mild acid sites exist on the surface of siliceous MCM-41. Chondhary

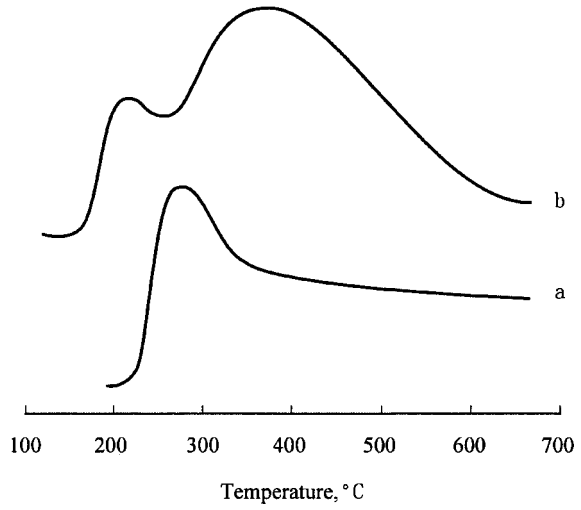


**FIG. 3.** $NH_3$-TPD profiles of (a) siliceous MCM-41 and (b) $\gamma$-$Al_2O_3$.

*et al.* characterized siliceous MCM-41 by means of $^1H$–$^{29}$ Si cross-polarization magic-angle spinning NMR and IR. They reported the presence of a large number of terminal SiOH groups on the surface (12). It is assumed that the mild acidity of siliceous MCM-41 may be attributed to these SiOH groups.

### *3.2. HDS of DBT*

A model fuel containing 1 wt% DBT in decalin was used to investigate the HDS activities for Ni–Mo sulfide catalysts supported over siliceous MCM-41. Fig. 4 shows the

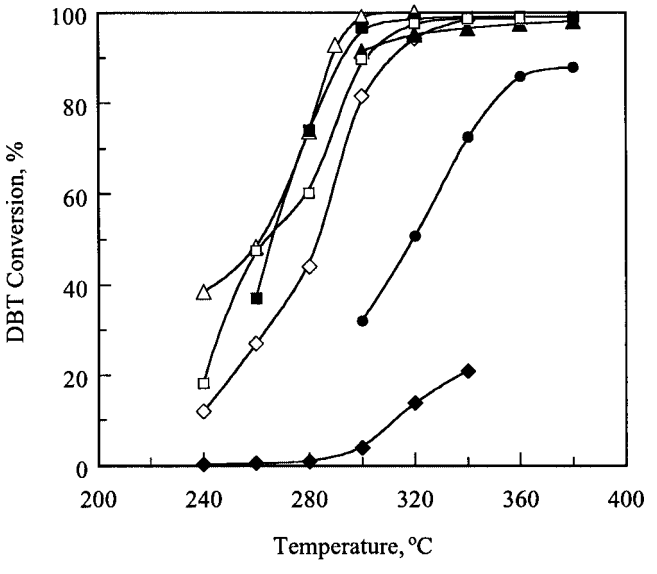


**FIG. 4.** Variation of DBT conversion with temperature during HDS catalyzed by siliceous MCM-41-supported Ni–Mo sulfides: (◆), Ni/MCM-41; (●), Mo/MCM-41; (◇), Ni–Mo(0.25); (▲), Ni–Mo(0.50); (△), Ni–Mo(0.75); (■), Ni–Mo(1.00); (□), Ni–Mo(1.25).

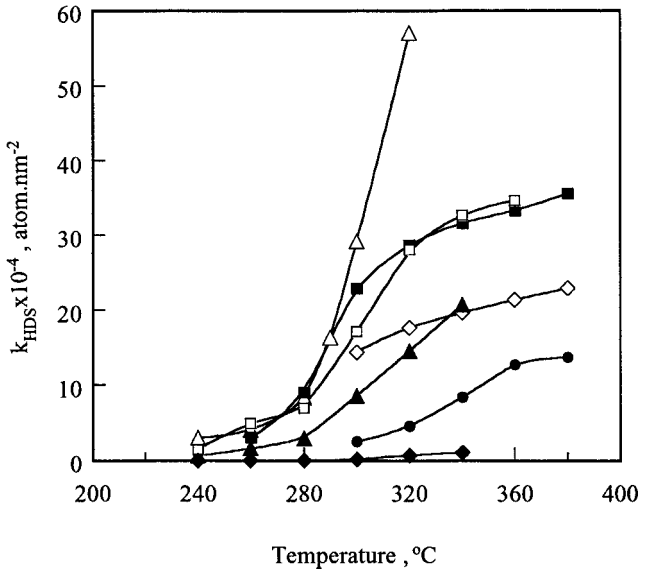


**FIG. 5.** Variation of HDS reaction constant with temperature during HDS catalyzed by siliceous MCM-41-supported Ni–Mo sulfides: (◆), Ni/MCM-41; (●), Mo/MCM-41; (◇), Ni–Mo(0.25); (▲), Ni–Mo(0.50); (△), Ni–Mo(0.75); (■), Ni–Mo(1.00); (□), Ni–Mo(1.25).

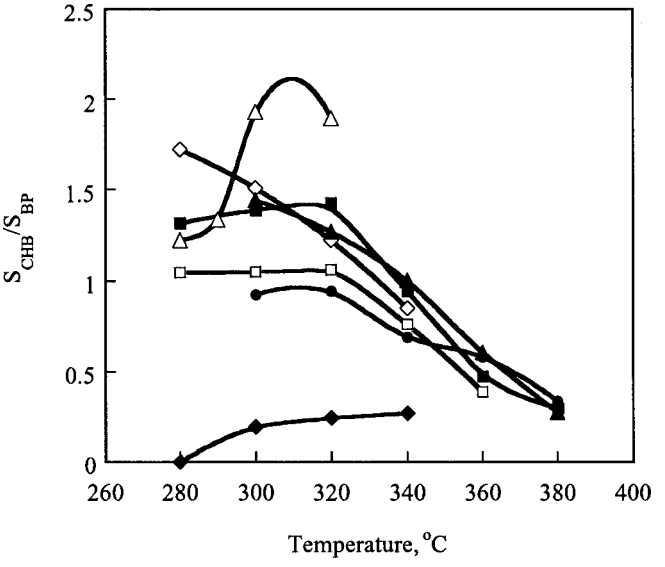


**FIG. 6.** Variation of $S_{CHB}/S_{BP}$ with temperature during HDS catalyzed by siliceous MCM-41-supported Ni–Mo sulfides: (◆), Ni/MCM-41; (●), Mo/MCM-41; (◇), Ni–Mo(0.25); (▲), Ni–Mo(0.50); (△), Ni–Mo(0.75); (■), Ni–Mo(1.00); (□), Ni–Mo(1.25).

conversion of DBT during HDS catalyzed by Ni–Mo/MCM-41 as a function of temperature, compared with Ni/MCM-41 (NiO 20 wt%) and Mo/MCM-41 ($MoO_3$ 20 wt%). The change of HDS reaction rate with temperature for this series of catalysts is shown in Fig. 5. All the Ni–Mo catalysts showed substantially high activity for converting DBT into hydrocarbons. Similar to Co–Mo/MCM-41 catalysts (7), maximum activity was observed for the Ni–Mo/MCM-41 catalyst at a Ni/Mo atomic ratio of 0.75.

The reaction constants of HDS, HGY, HYD, and HYC at temperatures of 300 and 320°C are summarized in Table 3. In contrast with Co–Mo/MCM-41 catalysts (7), HYD is greatly enhanced for Ni–Mo/MCM-41 catalysts; the rate of HYD exceeds that of HGY. Moreover, it is observed that the HYC rate increases with the HYD rate.

The ratio of CHB selectivity to BP selectivity ($S_{CHB}/S_{BP}$) is plotted against HDS reaction temperature for MCM-41-supported Mo, Ni, and Ni–Mo catalysts, as shown in Fig. 6. All the Ni–Mo/MCM-41 catalysts yield a higher $S_{CHB}/S_{BP}$ ratio than either Mo/MCM-41 or Ni/MCM-41, suggesting that there exists a synergetic effect between Ni and Mo sulfides on the HYD path during HDS.

The $S_{CHB}/S_{BP}$ ratio for the Ni/MCM-41 catalyst is higher than that for Co/MCM-41 (7) but is lower than that for Mo/MCM-41. Moreover, the $S_{CHB}/S_{BP}$ ratio decreases with the reaction temperature for all the MCM-41-supported catalysts except for Ni/MCM-41. These results suggest that the lower desulfurization activity of Ni species leads to the lower $S_{CHB}/S_{BP}$ ratio for Ni/MCM-41 even though Ni species are much more active than Mo species in hydrogenation.

**TABLE 3**

**Reaction Constants for HDS, HYD, HYG, and HYC during HDS of DBT Catalyzed by Ni–Mo/MCM-41**

| Catalyst | $MoO_3$ | Ni–Mo (0.25) | Ni–Mo (0.50) | Ni–Mo (0.75) | Ni–Mo (1.00) | Ni–Mo (1.25) | NiO |
|---|---|---|---|---|---|---|---|
| 300°C | | | | | | | |
| $k_{HDS}$($\times10^{-4}$ atom/nm$^2\cdot$s) | 2.52 | 8.59 | 14.36 | 29.16 | 22.92 | 17.10 | 0.19 |
| $k_{HYG}$($\times10^{-4}$ atom/nm$^2\cdot$s) | 1.00 | 2.48 | 4.67 | 6.76 | 6.76 | 5.66 | 0.16 |
| $k_{HYD}$($\times10^{-4}$ atom/nm$^2\cdot$s) | 0.93 | 3.75 | 6.73 | 13.06 | 9.40 | 5.95 | 0.03 |
| $k_{HYC}$($\times10^{-4}$ atom/nm$^2\cdot$s) | 0.29 | 1.18 | 1.48 | 4.66 | 3.38 | 2.74 | 0.00 |
| 320°C | | | | | | | |
| $k_{HDS}$($\times10^{-4}$ atom/nm$^2\cdot$s) | 4.61 | 14.54 | 17.65 | 57.01 | 28.68 | 28.06 | 0.69 |
| $k_{HYG}$($\times10^{-4}$ atom/nm$^2\cdot$s) | 1.71 | 4.52 | 5.75 | 9.98 | 6.20 | 7.77 | 0.29 |
| $k_{HYD}$($\times10^{-4}$ atom/nm$^2\cdot$s) | 1.61 | 5.52 | 7.71 | 18.93 | 8.83 | 8.25 | 0.07 |
| $k_{HYC}$($\times10^{-4}$ atom/nm$^2\cdot$s) | 0.65 | 2.25 | 2.29 | 14.05 | 6.83 | 6.02 | 0.32 |

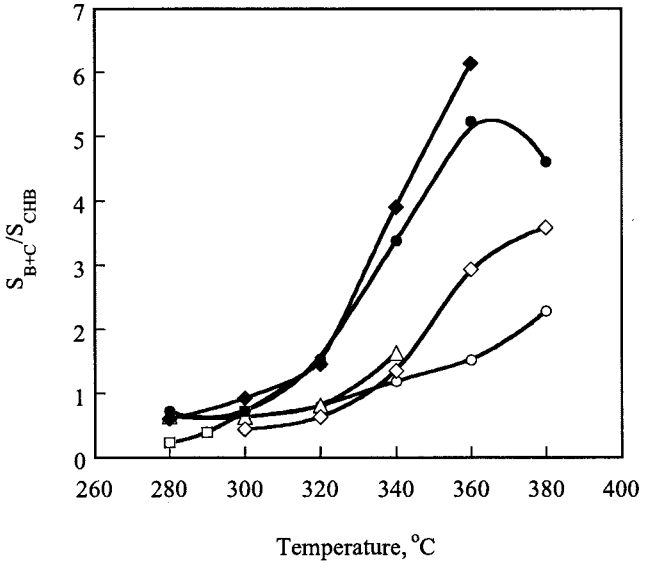


**FIG. 7.** Variation of $S_{B+C}/S_{CHB}$ with temperature during HDS catalyzed by siliceous MCM-41-supported Ni–Mo sulfides: (●), Mo/MCM-41; (◇), Ni–Mo(0.25); (▲), Ni–Mo(0.50); (△), Ni–Mo(0.75); (■), Ni–Mo(1.00); (□), Ni–Mo(1.25).

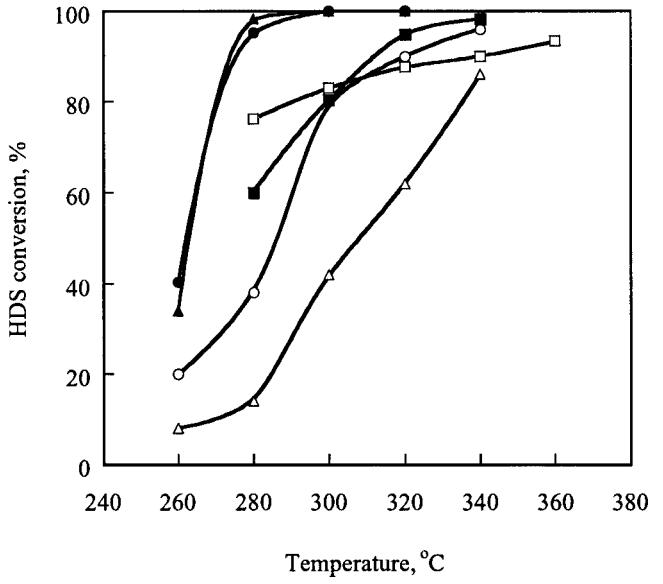


**FIG. 8.** Variation of HDS conversion with temperature during HDS of 4-MDBT (●, ○), 4,6-DMDBT (▲, △), and high-sulfur diesel (■, □). Solid: Ni–Mo(0.75), open: commercial deep HDS catalyst.

The variation of the ratio of benzene–cyclohexane selectivity to CHB selectivity ($S_{B+C}/S_{CHB}$) with temperature is shown in Fig. 7. The $S_{B+C}/S_{CHB}$ ratio increases with reaction temperature for all the Ni–Mo/MCM-41 catalysts, suggesting that the decomposition of CHB into benzene and cyclohexane is enhanced at high temperatures.

### *3.3. HDS of 4-MDBT, 4,6-DMDBT, and Diesel*

It is believed that alkyl dibenzothiophenes substituted by alkyl groups at the 4 and/or 6 position are the most refractory sulfur-containing molecules due to the increased steric hindrance (13). To evaluate the performance of the prepared Ni–Mo/MCM-41 HDS catalysts, Ni–Mo(0.75) was chosen to investigate the HDS of 4-MDBT (0.5 wt% in decalin), 4,6-DMDBT (0.5 wt% in decalin), and a high-sulfur-containing straight-run diesel (S 2.83 wt%). The variation of HDS conversion with temperature for different feeds is illustrated in Fig. 8, compared with a commercial deep HDS catalyst. It is shown that the Ni–Mo(0.75) catalyst exhibited excellent performance in desulfurizing the more refractory DBT derivatives and the high-sulfur-containing diesel, superior to that of the commercial catalyst.

### *3.4. Sulfur Behavior during HDS by Isotope Tracer Method*

The dynamic behavior of the sulfur atom during HDS of DBT was investigated by the $^{35}S$ isotope tracer technique. The HDS of DBT was conducted over sulfided Ni–Mo(0.75) catalyst at 280°C and 5.0 MPa. A typical profile of radioactivity vs reaction time is illustrated in Fig. 9. A decalin solution of 1 wt% [$^{32}$S]DBT was pumped into the reactor to start the HDS reaction. After the conversion of [$^{32}$S]DBT became constant, a flow of 1 wt% [$^{35}$S]DBT in decalin was introduced into the reactor to replace the [$^{32}$S]DBT solution. The radioactivity of the unreacted [$^{35}$S]DBT in the liquid product increased and approached a steady state immediately after the introduction of [$^{35}$S]DBT, whereas there was a delay for the radioactivity of the released [$^{35}$S]$H_2S$

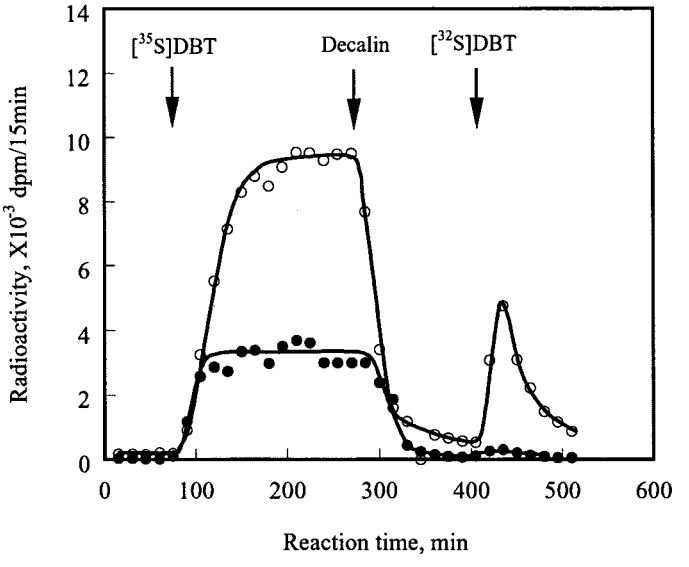


**FIG. 9.** Changes in radioactivities of unreacted [$^{35}$S]DBT (●) and released [$^{35}$S]$H_2S$ (○) with reaction time during HDS of DBT at 280°C and 5.0 MPa.

to reach a steady state. After both the radioactivity of the unreacted [$^{35}$S]DBT and that of the released [$^{35}$S]$H_2S$ became constant, a flow of decalin was introduced to replace the [$^{35}$S]DBT solution. Both the radioactivity of unreacted [$^{35}$S]DBT and that of released [$^{35}$S]$H_2S$ decreased sharply. Little [$^{35}$S]DBT was detected during the period of purging with decalin and hydrogen, suggesting that there was no $H_2S$ physically absorbed on the surface of the catalyst. After a long period of purging, a flow of 1 wt% [$^{32}$S]DBT solution was introduced again to replace decalin. No noticeable radioactivity change was detected in the liquid product, but a peak of $^{35}$S radioactivity in the gas phase appeared in the form of [$^{35}$S]$H_2S$. The profile of Ni–Mo/MCM-41 is similar to that of Co–Mo/MCM-41 (7), suggesting that the reaction cycle on either catalyst is the same.

## 4. DISCUSSION

### *4.1. HDS*

It is well accepted that high dispersion of Ni (Co)–Mo species on the support surface is essential for preparation of high-performance HDS catalysts and that the surface properties, such as acidity, affect the dispersion and the local environment of the metal species. In a previous paper (7), we reported that siliceous MCM-41-supported Co–Mo sulfide catalysts exhibited very high activity for DBT HDS. It is assumed that the high surface area and the mild acidity of the support may lead to a high dispersion of the metal species on the surface.

It is illustrated in Figs. 4 and 5 that Ni–Mo/MCM-41 also performed excellently in the HDS of DBT. Moreover, the more refractory polyaromatic sulfur molecules such as 4-MDBT and 4,6-DMDBT can be easily desulfurized by the prepared Ni–Mo/MCM-41 (0.75) catalyst. This catalyst also shows high performance in HDS of a high-sulfur diesel. Similar to Co–Mo/MCM-41, the large surface area of the support may contribute subtantially to the high HDS activity.

It is interesting to note that the $S_{CHB}/S_{BP}$ ratio for Ni/MCM-41 is equivalent to that for Co/MCM-41, but lower than that for Mo/MCM-41. Since the HYD path of HDS involves two steps, i.e., hydrogenation of one phenyl ring and desulfurization, the lower desulfurization ability of Ni or Co species may lead to the lower selectivity of cyclohexylbenzene even though it has high hydrogenation activity. However, the $S_{CHB}/S_{BP}$ ratio for Ni–Mo/MCM-41 is higher than that for Mo/MCM-41 or Co–Mo/MCM-41, and a remarkable synergetic effect for the HYD path is observed for Ni–Mo/MCM-41. The electronic transfer between Ni and Mo is assumed to be the key factor in the synergetic effect (14, 15).

In contrast with Co–Mo/MCM-41, the HYD path dominates over the HGY path in the HDS of DBT over Ni–Mo/MCM-41. According to a review by Whitehurst (13), the rate constant of HDS after hydrogenation of one ring is 33 times that of HGY for Co- or Ni-promoted Mo sulfide catalyst. However, the rate constant of HYD of the DBT phenyl ring is much lower than that of HGY of Co–Mo sulfides, limiting the rate of the HYD path. Consequently, the synergetic effect of Ni–Mo sulfides may account for the higher HDS activity of Ni–Mo/MCM-41 for DBT and its derivatives. Moreover, it is observed that $S_{CHB}/S_{BP}$ decreases with increasing reaction temperature while $S_{B+C}/S_{CHB}$ increases considerably with increasing temperature. It is assumed that HYC of CHB is accelerated at high reaction temperatures.

### *4.2. Mechanism of HDS over Ni–Mo/MCM-41 Catalysts*

In the development of high-performance deep-HDS catalysts, much attention has been focused on the theoretical aspects of the active phase on the surface to provide a guide for constructing active sites. Nevertheless, the catalytic circle of HDS reaction on the active sites should be clarified.

To elucidate the catalytic circle of HDS reaction over Ni–Mo/MCM-41, the $^{35}$S isotope tracer experiment was carried out during HDS of DBT. The sulfur atoms removed from DBT molecules were not released directly into gas phase as $H_2S$ but were retained on the surface of the catalyst, similarly to the results for Co–Mo/MCM-41 (7). Since purging with decalin in the presence of $H_2$ could not remove the retained sulfur atoms on the catalyst, it is unlikely that the retained $^{35}$S exists in the form of adsorbed $H_2S$ on the surface. On the other hand, these sulfur atoms could be released by the introduction of new DBT molecules, indicating that sulfur-atom exchange between DBT molecules and sulfur species on the surface of the catalyst may be involved during HDS of DBT and the sulfur atoms on the surface may serve as active sites.

In contrast with Co–Mo/MCM-41 catalysts, the HYD path of HDS catalyzed by Ni–Mo/MCM-41 contributes more to the conversion of DBT than the HGY path. It is assumed that the enhancement of the HYD path may be attributed to the strong hydrogenation ability of Ni species, and it is proposed that hydrogenation occurs on other sites (such as Ni metal) while the removal of the sulfur atom from the thiophenic ring takes place on the NiMoS clusters and the catalytic circle is the same as that for Co–Mo/MCM-41 catalysts.

Based on DFT calculation, Neurock suggested that thiophene absorbs in the $\eta 4$ mode at low coverage of metal species and in the $\eta 1$ mode at high coverage (16). The coordination structure of $Ni_3S$ and an overall catalytic cycle in the HDS of thiophene were also depicted and are in accordance with experimental results. Accordingly, we assumed that Ni, Mo, and S atoms in the supported binary sulfides did not coordinate in a line on the surface but as dimers. A catalytic circle during HDS over sulfided Ni–Mo catalysts

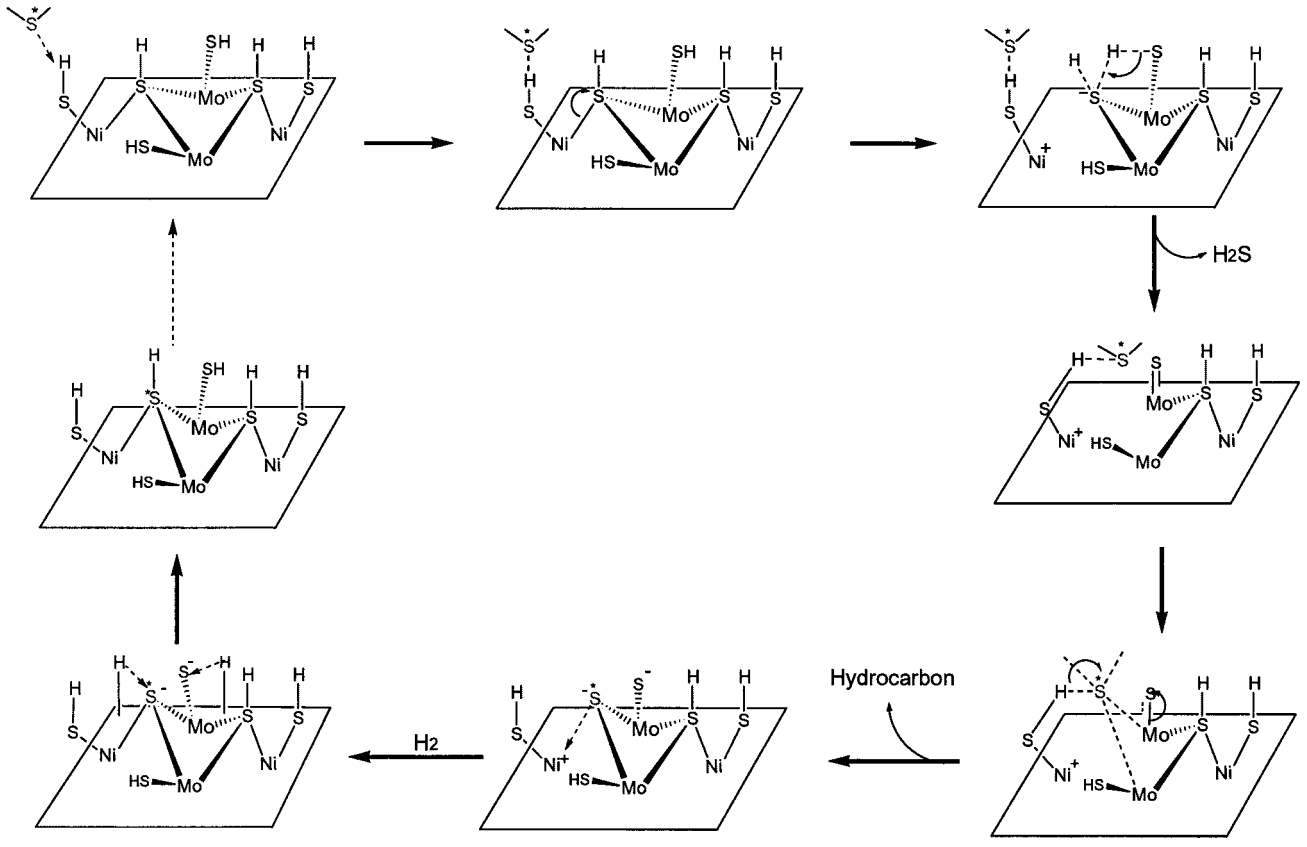


**SCHEME 1.** Catalytic circle in HDS of thiophenic sulfur-containing molecules catalyzed by supported Ni–Mo sulfides.

was proposed, as shown in Scheme 1. The mechanism briefly describes the possible reaction steps involved on the local site. It was assumed that gaseous hydrogen adsorbed dissociatively on the surface of catalysts and that the hydrogen species consumed in the reaction were supplemented by means of spillover on the surface (17).

Based on the theoretical calculation, Harris and Chianelli concluded that Co or Ni donate electrons to Mo to enhance the HDS activity. The electron donation involves an electron transfer from a Co–S or Ni–S antibonding orbital to a Mo–S antibonding orbital (15). When a sulfur-containing molecule absorbs on the sulfide cluster in the $\eta 1$ mode through hydrogen bonding, cluster reconstruction occurs to accommodate the incoming molecule: the Ni–S bond is cleaved and the three-fold bound sulfur moves to form a two-fold bond. Since the two-fold bound sulfur is unstable, it is eliminated with the absorbed hydrogen species to form $H_2S$, leaving a positive-charged "vacancy." The sulfur atom in the molecule will occupy the vacancy, forming a new sulfur bridging bond and breaking the sulfur bonds in the molecule to form a hydrocarbon. With the desorption of the hydrocarbon, the new sulfur bridging bond moves to form the three-fold bond and the structure of the cluster returns. When a new sulfur-containing molecule absorbs on the cluster, a new catalytic circle begins.

The sulfur-containing molecule represents a thiophenic molecule such as thiophene, benzothiophene, dibenzothiophene, their alkyl-substituted derivatives, and their hydrogenated intermediates. In addition, it is assumed that the sulfur-containing molecule could be $H_2S$ formed during HDS. $H_2S$ may be involved in the catalytic circle, as evidenced by the broadening and tailing of the output peak in the pulse tracer experiment during HDS (7). The competitive adsorption of $H_2S$ results in a slowdown of the overall HDS reaction rate.

## 5. CONCLUSION

In summary, high-performance deep-HDS catalysts were obtained by supporting Ni–Mo species on siliceous MCM-41. The highest HDS activity was observed at a Ni/Mo atomic ratio of 0.75 for this series of catalysts, similar to that of Co–Mo/MCM-41(7). Ni–Mo(0.75)/MCM-41 exhibited excellent performance in the HDS of 4-MDBT, 4,6-DMDBT, or high-sulfur diesel. TPR data revealed that the $H_2$-consumption peak at low temperature shifted to lower temperature when the Ni/Mo atomic ratio increased. In addition, the $H_2$-consumption peak at low temperature split into two or three peaks when the Ni/Mo atomic ratio was in the vicinity of 0.75, indicating that some intermediate

species were formed. It is assumed that the shifting and splitting of the reduction peak is attributed to the interaction between metal species and the support and to the synergetic effect of the binary metal species.

In contrast with the Co–Mo/MCM-41 catalysts, the HYD path out performs the HGY path in the HDS of DBT catalyzed by Ni–Mo/MCM-41. Ni species contribute to the improved HDS activity mainly by accelerating hydrogenation of a phenyl ring in DBT. It seems that high reaction temperature accelerates the cracking of CHB into benzene and cyclohexane. The $^{35}S$ istope tracer experiment results suggest that sulfur-atom exchange between sulfur-containing molecules and the active sites on the surface is involved in the HDS reaction. Accordingly, a reaction mechanism for HDS was proposed.

## ACKNOWLEDGMENTS

This research was partly supported by the Natural Science Foundation of China (20003002) and by the Young Promising Teachers' Funds from the Education Ministry of China. The authors are grateful to Mr. X. Li, Mr. D. Han, Mr. S. Otsuki, Mr. H. Shirai, Mr. H. Sukuno, Mr. Putu, and Mr. Saito for their kind help in the research work.

## REFERENCES

1. Beck, J. S., Vartuli, J. C., Roth, W. J., Leonowicz, M. E., Kresge, C. T., Schmitt, K. D., Chu, C. T.-W., Olson, D. H., Sheppard, E. W., McCullen, S. B., Higgins, J. B., and Schlenker, J. L., *J. Am. Chem. Soc.* **114**, 10834 (1992).
2. Corma, A., Martínez, A., Martínez-Soria, V., and Montón, J. B., *J. Catal.* **153**, 25 (1995).
3. Song, C. S., and Reddy, K. M., *Appl. Catal. A* **176**(1), 1 (1999).
4. Reddy, K. M., Wei, B., and Song, C., *Catal. Today* **43**(3–4), 261 (1998).
5. Landau, M. V., Vradman, L., Herskowitz, M., Koltypin, Y., and Gedanken, A., *J. Catal.* **201**(1), 22 (2001).
6. Ramíre, I., Contreras, R., Castillo, P., Klimova, T., Zárate, R., and Luna, R., *Appl. Catal., A* **197**, 69 (2000).
7. Wang, A., Wang, Y., Kabe, T., Chen, Y., Ishihara, A., and Qian, W., *J. Catal.* **199**, 19 (2001).
8. Wang, A., Li, X., Chen, Y., Han, D., Wang, Y., Hu, Y., and Kabe, T., *Chem. Lett.* **5**, 474 (2001).
9. Campaigne, E., Hewitt, L., and Ashby, J., *J. Heterocycl. Chem.* **6**, 553 (1969).
10. Gerdil, R., and Lucken, E. A. C., *J. Am. Chem. Soc.* **87**, 213 (1965).
11. Navarro, R., Pawelec, B., Fierro, J. L. G., and Vasudevan, P. T., *Appl. Catal.*, *A* **148**, 23 (1996).
12. Chondhary, V. R., and Kshudiram, M., *Langmuir* **16**(21), 8024 (2000).
13. Whitehurst, D. D., Isoda, T., and Mochida, I., *Adv. Catal.* **42**, 345 (1998).
14. Cattenot, M., Geantet, C., Glasson, C., and Breysse, M., *Appl. Catal., A* **213**, 217 (2001).
15. Harris, S., and Chianelli, R. R., *J. Catal.* **98**, 17 (1986).
16. Neurock, M., *Appl. Catal., A* **160**, 169 (1997).
17. Nagai, M., Koyama, H., Sakamoto, S., and Omi, S., *Stud. Surf. Sci. Catal.* **127**, 195 (1999).